Journal of ELECTRONIC MATERIALS, Vol. 37, No. 8, 2008
DOI: 10.1007/s11664-008-0484-6

Regular Issue Paper

Electrical Characteristics and Photoresponse of ZnO/ZnTe Heterojunction Diodes

W. WANG,[1,2] A. LIN,[1] and J.D. PHILLIPS[1]

1.—Department of Electrical Engineering and Computer Science, The University of Michigan, Ann Arbor, MI 48109-2122, USA. 2.—e-mail: umwwm@umich.edu

Heterojunction diodes consisting of *n*-type ZnO and *p*-type ZnTe were grown by pulsed laser deposition and molecular beam epitaxy, respectively, on GaAs (001) substrates. Strong diode rectifying behavior was observed in the current–voltage characteristics with a current on/off ratio of $J_{on}/J_{off} = 1 \times 10^5$ and a diode ideality factor of $n = 1.5$. A strong photoresponse in the energy range of 2.3 eV to 3.6 eV was observed, corresponding to the bandgap energies of ZnTe and ZnO, respectively. A photovoltaic response was observed with a relatively small fill factor with a short-circuit current $J_{sc} \sim 0.8$ mA/cm^2 and open-circuit voltage of $V_{oc} \sim 60$ mV subject to illumination by a tungsten lamp. The photovoltaic response and reverse saturation current are believed to be limited by defects related to the mismatch between the ZnTe and ZnO structures and defects in the ZnO layer deposited at low temperature. The spectral response of the diodes is modeled with a close match to experimental measurements.

Key words: Heterojunction, ZnO, ZnTe

INTRODUCTION

ZnO shows tremendous potential for visible/ultraviolet optoelectronic devices including light-emitting diodes, lasers, and photodetectors. However, the realization of these devices based on ZnO is impeded by the inability to reliably and/or reproducibly achieve *p*-type conductivity. The low formation energy of *n*-type native defects including Zn interstitials, O vacancies, and unintentional donors such as hydrogen leads to high background *n*-type carrier concentrations.[1] In addition to controlling the background concentration, *p*-type doping is difficult in ZnO due to deep acceptor energies for substitutional impurities or the compensating nature of acceptor defect complexes. There has been great progress over the past several years in the achievement of *p*-type ZnO through a number of demonstrations,[2–10] though a reliable and reproducible technique for *p*-type doping of ZnO has yet to be identified. Conversely, ZnTe is a wide-bandgap II–VI compound semiconductor that is intrinsically *p*-type due to native defects in this material.[11] High-conductivity *p*-type ZnTe has also been established by nitrogen doping[12–15] with hole concentrations near 1×10^{20} cm^{-3}. Heterojunction diodes utilizing *p*-type ZnTe and *n*-type ZnO may present an opportunity for ZnO optoelectronic devices[16] or cadmium-free thin-film solar cells. Furthermore, electronic devices based on ZnO requiring an interface to *p*-type material may also be enabled, including bipolar transistors and junction field-effect transistors. In this work, *n*-ZnO/*p*-ZnTe heterojunction diodes on GaAs substrates are demonstrated. The electrical properties and related photoresponse are presented and compared with numerical simulation.

EXPERIMENT

Layers of ZnTe were grown by molecular beam epitaxy (MBE) on conducting *p*-type GaAs (001) substrates at a substrate temperature of 250°C. A heavily doped buffer layer with a thickness of

(Received March 18, 2008; accepted May 1, 2008; published online June 6, 2008)

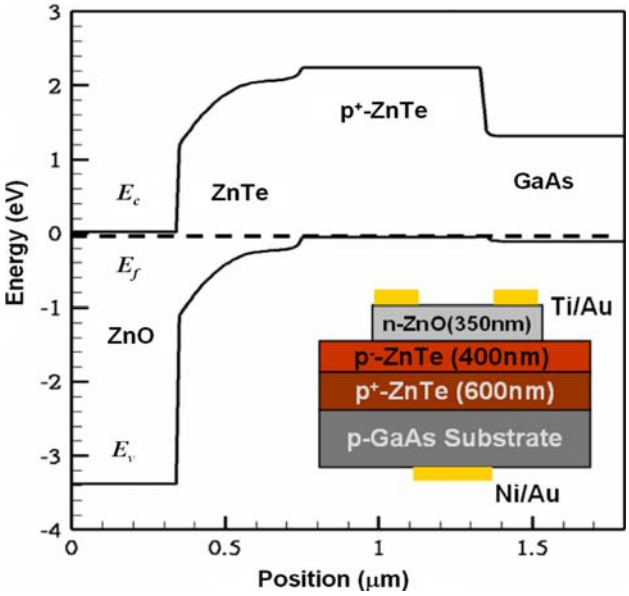

Fig. 1. Calculated energy band diagram at equilibrium and (*inset*) schematic device structure of the ZnO/ZnTe/GaAs heterojunction diode.

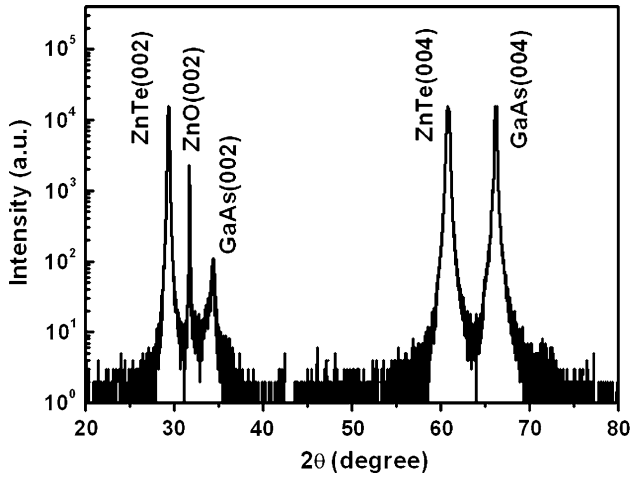

Fig. 2. X-ray diffraction θ–2θ scan of the ZnO/ZnTe heterojunction on GaAs (001).

0.6 μm was first grown by nitrogen doping with a nitrogen plasma source with an approximate hole concentration of 1×10^{19} cm^{-3}. A 0.4-μm-thick layer of ZnTe was grown without intentional doping. Independent calibration runs of ZnTe on insulating substrates resulted in background carrier concentrations of less than 10^{15} cm^{-3}. A subsequent layer of ZnO was grown by pulsed laser deposition (PLD) in a separate chamber, with a thickness of 350 nm. The substrate temperature for ZnO deposition was kept intentionally low at 200°C to avoid possible degradation of the ZnTe material. The electron concentration of ZnO grown under these conditions has been determined to be approximately 2×10^{18} cm^{-3}. Ti/Au 30 nm/70 nm for contacts to *n*-type ZnO and Ni/Au 50 nm/100 nm for bottom contacts to *p*-type GaAs were formed. The resulting device structure and equilibrium energy band diagram (band offsets are assumed to follow the electron affinity model) are shown in Fig. 1.

RESULTS AND DISCUSSION

X-ray diffraction (XRD) with ω–2θ wide-angle scanning, shown in Fig. 2, was used to examine the crystalline structure of the ZnO/ZnTe heterojunction. The ZnTe (002) and (004) reflections clearly indicate the predicted zincblende ZnTe (001) orientation on the GaAs (001) substrate. A strong ZnO (0002) reflection is observed, indicating the wurtzite *c*-plane ZnO (0001) orientation. Despite the apparent epitaxial relationship between ZnO, ZnTe, and GaAs, a significant defect density is likely in these heterojunctions due to the differing symmetry of the hexagonal ZnO crystal structure in comparison to zincblende ZnTe. Furthermore, a large defect density is also predicted for the large lattice mismatch in this orientation, where the crystalline relation (0001)ZnO//(001)ZnTe and [10$\bar{1}$0]ZnO//[110]ZnTe results in a lattice mismatch of 25%.

Room-temperature current–voltage (*I*–*V*) characteristics of the *n*-ZnO/*p*-ZnTe heterojunction are presented in Fig. 3a on both a logarithmic and linear scale. The leakage current for the diodes is $<5 \times 10^{-5}$ A (3 mA/cm^2) at a reverse bias of 5 V, with a breakdown voltage of approximately 10 V. In forward bias, the turn-on voltage is approximately 1 V, resulting in a current on/off ratio of J_{on}/J_{off} of approximately 1×10^5. The *I*–*V* characteristics in forward bias fit closely to the diode equation, $J = J_s \exp(qV - qJR_s/nkT)$, where J_s is the saturation current density, q is the charge of an electron, kT is the thermal energy, n is the ideality factor, and R_s is the series resistance. The ideality factor of the diode is determined to be 1.5 for the voltage range from 0 V to 0.5 V, indicating primarily diffusion current rather than generation–recombination current in the depletion region. Series resistance was determined to be $R_s = 0.034\ \Omega\ \text{cm}^2$.

A strong photoresponse is observed under illumination through a tungsten lamp with an estimated power density about 70 mW cm^{-2} through a microscope objective, as shown in Fig. 3b. A photovoltaic effect is observed under zero and forward bias, where a short-circuit current of $J_{sc} \sim 0.8$ mA/cm^2 and an open-circuit voltage of $V_{oc} \sim 60$ mV are observed. According to the relation $V_{oc} = nkT\ln(J_{sc}/J_s)/q$,[17] the small V_{oc} is related to a large reverse saturation current density. The reverse saturation current in these diodes may be related to defects arising from the mismatch between the ZnO and ZnTe crystalline structures or defects in the ZnO related to the low-temperature deposition process. We have also evaluated ZnO/ZnTe diodes with a similar structure, but without the heavily doped

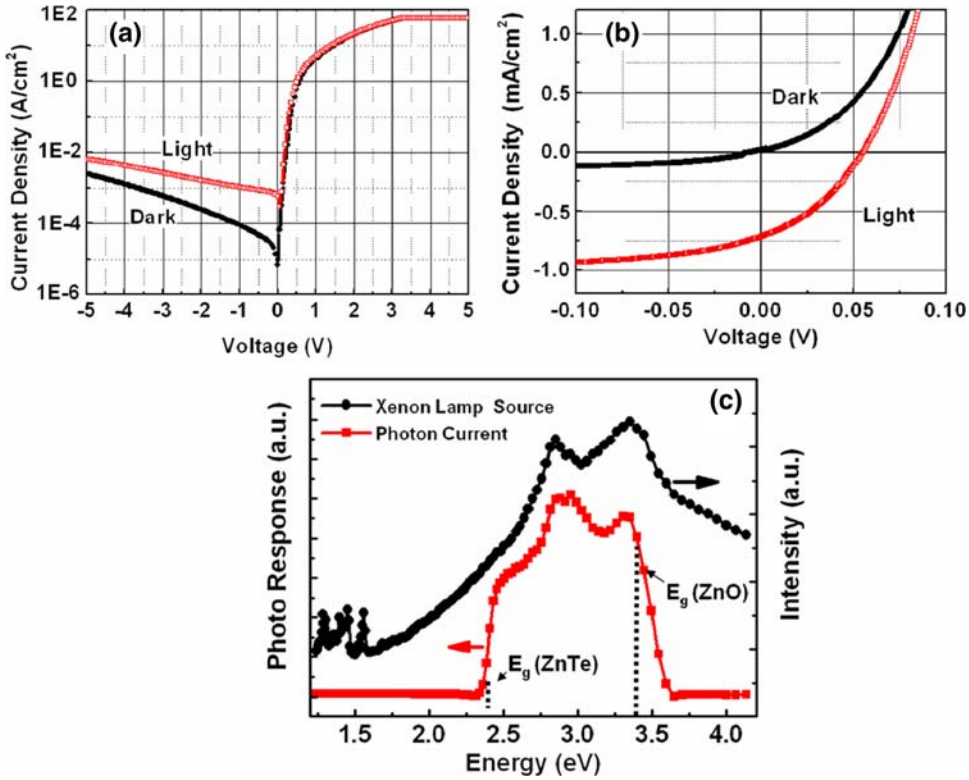

Fig. 3. Current–voltage characteristics for the ZnO/ZnTe heterojunction diode with and without illumination shown on (a) a logarithmic and (b) a linear scale. (c) Spectral response of the ZnO/ZnTe heterojunction diode and incident xenon lamp.

ZnTe buffer layer. The absence of the ZnTe buffer layer would be expected to result in a high density of dislocations within or near the diode depletion region, corresponding to the mismatched ZnTe/GaAs interface. These devices exhibited an increased ideality factor of $n = 1.9$ and lack of photovoltaic effect, consistent with these expectations. Two differing approaches may be used to reduce the reverse saturation current and increase the photovoltaic response. To improve the ZnTe/ZnO match, the (111) ZnTe orientation may be used for an improved match to the hexagonal symmetry of ZnO. Higher-quality ZnO material may be utilized by inverting the device structure, i.e., by growing ZnTe (requiring low-temperature growth) on high-quality ZnO, where (111) ZnTe growth would be expected.

The spectral response of the diodes is shown in Fig. 3c, where response between 2.3 eV and 3.6 eV is observed. There is clearly no significant response for energies below 2.3 eV, corresponding to the ZnTe bandgap energy. This observation indicates that the GaAs substrate does not play a role in determining the observed diode behavior. For incident photons with energy between the ZnTe and ZnO bandgap energies, absorption and carrier generation occurs primarily in the unintentionally doped ZnTe layer. This ZnTe layer will lie in the depletion region of the diode where photogenerated electron-hole pairs will be separated and collected across the junction by the built-in electric field. The spectral response cutoff at short wavelength (~3.6 eV) roughly corresponds to the ZnO bandgap energy, and is discussed in the following. When the energy of incident photons exceeds the band edge of ZnO (3.37 eV), there will be strong optical absorption in the ZnO layer. Shorter wavelengths will lead to increased absorption near the ZnO surface due to the increasing optical absorption coefficient at higher energies. In order for these photogenerated carriers to contribute to detector photocurrent, the minority carrier holes in the ZnO must diffuse to the junction in order to be swept to the *p*-side of the junction. However, the diffusion length of holes in ZnO is predicted to be only ~50 nm due to the short minority-carrier (hole) lifetime in *n*-ZnO, ~1 ns,[18] and low minority-carrier mobility, ~1 cm^2/Vs.[19] This hole diffusion length is significantly smaller than the thickness of the ZnO layer (350 nm) in the device structure. The short-wavelength cutoff of the detector response just above the ZnO band edge may be attributed to the long diode structure relative to the hole diffusion length.

A device model was used to validate our explanation for the photoresponse behavior. The photon generation rate as a function of position was calculated by $G(x) = \Phi_{opt}\alpha \exp(-\alpha x)$, where x is the position departing from the surface, Φ_{opt} is the incident photon flux, and α is the absorption coefficient. The absorption coefficient is given by the following expressions near the band edge[20]

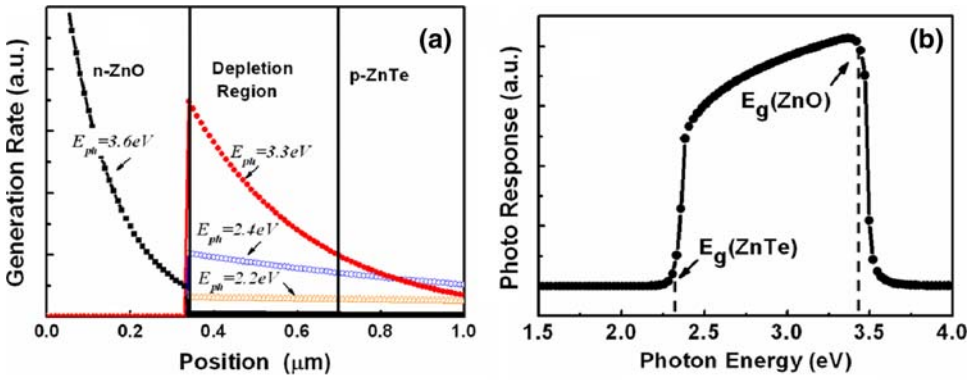

Fig. 4. Simulation results for the ZnTe/ZnO heterojunction diode showing (a) the position-dependent carrier generation rate at varying incident photon energy and (b) the spectral response.

$$\alpha = \alpha_0 \exp\left(\frac{E_{\mathrm{ph}} - E_{\mathrm{g}}}{kT}\right), \quad E_{\mathrm{ph}} < E_{\mathrm{g}} \tag{1}$$

$$\alpha = \alpha_0 + \alpha_1 \sqrt{\frac{E_{\mathrm{ph}} - E_{\mathrm{g}}}{kT}}, \quad E_{\mathrm{ph}} > E_{\mathrm{g}}, \tag{2}$$

where E_g is the bandgap of the semiconductor, E_{ph} is the incident photon energy, and α_0 and α_1 are fitting parameters for the optical absorption coefficient. The values for these fitting parameters are assumed to be $\alpha_0 \sim 5 \times 10^4$ cm^{-1}, $\alpha_1 \sim 1 \times 10^4$ cm^{-1}, for ZnO,[21] and $\alpha_0 \sim 5000$ cm^{-1}, $\alpha_1 \sim 1000$ cm^{-1} for ZnTe.[22] The carrier generations at four energies in the range of 2.2 eV to 3.6 eV are presented in Fig. 4a. From this plot, a strong transition from photogeneration in the ZnTe to predominant photogeneration near the incident ZnO surface is observed with increasing photon energy. The photon current density is mainly proportional to the integral of $G(x)$ in hole diffusion length in the n region, the depletion region, and the electron diffusion length in p region. The resulting current density for the diode is then calculated according to drift-diffusion equations described in Ref. 23. The calculated spectral response due to white-light illumination with uniform intensity is then shown in Fig. 4b. The simulated spectral response is qualitatively in good agreement with the measured spectral response shown in Fig. 3. Deviations between calculated and measured spectral responses may be primarily attributed to the nonuniform spectral response of the xenon lamp and optical interference effects not accounted for in the simulation.

CONCLUSION

Strong rectifying diode behavior is observed for n-ZnO/p-ZnTe heterojunction diodes with $I_{on}/I_{off} \sim 1 \times 10^5$ and ideality factor n = 1.5. Strong photoresponse is observed in the range of 2.3 eV to 3.6 eV, where cutoff energies are determined by the absorption edge for ZnTe and minority hole collection in ZnO, respectively. The diode behavior and photovoltaic response indicates that these structures are promising for future electronic and optoelectronic devices based on ZnO heterojunctions, despite the mismatch between ZnTe and ZnO. Significant improvements to these heterojunction devices may be expected with improved high-temperature ZnO growth and combination of ZnTe (111) with ZnO (0001).

ACKNOWLEDGEMENTS

We would like to thank F. Yang for assistance with spectral response measurements. This work is supported by the Center for Optoelectronic Nanostructured Semiconductor Technologies, a DARPA UPR award HR0011-04-1-0040.

REFERENCES

1. D.C. Look, *Mater. Sci. Eng.* B80, 383 (2001). doi:10.1016/S0921-5107(00)00604-8.
2. A. Tsukazaki, A. Ohtomo, T. Onuma, M. Ohtani, T. Makino, M. Sumiya, K. Ohtani, S.F. Chichibu, S. Fuke, Y. Segawa, H. Ohno, H. Koinuma, and M. Kawasaki, *Nat. Mater.* 4, 42 (2005). doi:10.1038/nmat1284.
3. D.C. Look, G.M. Renlund, R.H. BurgenerII, and J.R. Sizelove, *Appl. Phys. Lett.* 85, 5269 (2004).
4. Y.R. Ryu, S. Zhu, D.C. Look, J.M. Wrobel, H.M. Jeong, and H.W. White, *J. Cryst. Growth* 16, 330 (2000).
5. D.C. Look, D.C. Reynolds, C.W. Litton, R.L. Jones, D.B. Eason, and G. Cantwell, *Appl. Phys. Lett.* 81, 1830 (2002).
6. A. Allenic, W. Guo, Y.B. Chen, Y. Che, Z.D. Hu, B. Liu, and X.Q. Pan, *J. Phys. D: Appl. Phys.* 41, 025103 (2008).
7. F.X. Xiu, Z. Yang, L.J. Mandalapu, D.T. Zhao, J.L. Liu, and W.P. Beyermann, *Appl. Phys. Lett.* 87, 152101 (2005).
8. Y.R. Ryu, T.S. Lee, and H.W. White, *Appl. Phys. Lett.* 83, 87 (2003).
9. K.-K. Kim, H.-S. Kim, D.-K. Hwang, J.-H. Lim, and S.-J. Park, *Appl. Phys. Lett.* 83, 63 (2003).
10. Y.W. Heo, Y.W. Kwon, Y. Li, S.J. Pearton, and D.P. Norton, *Appl. Phys. Lett.* 84, 3474 (2004).
11. R.S. Title, G. Mande, and F.F. Morehead, *Phys. Rev.* 136, 300 (1964).
12. S.O. Ferreira, H. Sitter, W. Faschinger, and G. Brunthaler, *J. Cryst. Growth* 140, 282 (1994).
13. J. Han, T.S. Stavrinides, M. Kobayashi, R.L. Gunshor, M.M. Hagerott, and A.V. Nurmikko, *Appl. Phys. Lett.* 62, 840 (1993).
14. I.W. Tao, M. Jurkovic, and W.I. Wang, *Appl. Phys. Lett.* 64, 1848 (1994).

15. C.M. Rouleau, D.H. Lowndes, J.W. McCamy, J.D. Budai, D.B. Poker, D.B. Geohegan, and A.A. Puretzky, *S. Zhu. Appl. Phys. Lett.* 67, 2545 (1995).
16. A.E. Tsurkan, N.D. Fedotova, L.V. Kicherman, and P.G. Pas'Ko, *Sov. Phys. Semcond.* 9, 786 (1975).
17. P. Bhattacharya, *Semiconductor Optoelectronic Devices* (New Jersey: Prentice Hall, 1994), p. 417.
18. K. Moazzami, T.E. Murphy, J.D. Phillips, M.C.-K. Cheung, and A.N. Cartwright, *Semicond. Sci. Technol.* 21, 717 (2006).
19. D.C. Look and B. Claflin, *Phys. Stat. Sol. (b)* 241, 624 (2004).
20. C.A. Hougen, *J. Appl. Phys.* 66, 3763 (1989).
21. V. Srikant and D.R. Clarke, *J. Appl. Phys.* 81, 6357 (1997).
22. A. Erlacher, M. Ambrico, G. Perna, L. Schiavulli, T. Ligonzo, H. Jaeger, and B. Ullrich, *Appl. Surf. Sci.* 248, 402 (2005).
23. H.J. Hovel, *Semiconductors and Semimetals: Solar Sells*, vol. II (Academic Press, New York, 1975), p. 17.